Journal of Solid State Chemistry 182 (2009) 27–36

Contents lists available at ScienceDirect

Journal of Solid State Chemistry

journal homepage: www.elsevier.com/locate/jssc

Effect of hydrothermal treatment on properties of Ni–Al layered double hydroxides and related mixed oxides

František Kovanda [a,*], Tomáš Rojka [a], Petr Bezdička [b], Květa Jirátová [c], Lucie Obalová [d], Kateřina Pacultová [d], Zdeněk Bastl [e], Tomáš Grygar [b]

[a] Department of Solid State Chemistry, Institute of Chemical Technology, Prague, Technická 5, 166 28 Prague, Czech Republic
[b] Institute of Inorganic Chemistry of the ASCR, v. v. i., 250 68 Řež, Czech Republic
[c] Institute of Chemical Process Fundamentals of the ASCR, v. v. i., Rozvojová 135, 165 02 Prague, Czech Republic
[d] Technical University of Ostrava, 17. listopadu 15, 708 33 Ostrava, Czech Republic
[e] J. Heyrovský Institute of Physical Chemistry of the ASCR, v. v. i., Dolejškova 3, 182 23 Prague, Czech Republic

ARTICLE INFO

Article history:
Received 20 June 2008
Received in revised form
12 September 2008
Accepted 20 September 2008
Available online 8 October 2008

Keywords:
Layered double hydroxides
Hydrotalcite-like compounds
Thermal decomposition
Nickel–aluminum mixed oxides
Porous structure
N_2O decomposition

ABSTRACT

The Ni–Al layered double hydroxides (LDHs) with Ni/Al molar ratio of 2, 3, and 4 were prepared by coprecipitation and treated under hydrothermal conditions at 180 °C for times up to 20 h. Thermal decomposition of the prepared samples was studied using thermal analysis and high-temperature X-ray diffraction. Hydrothermal treatment increased significantly the crystallite size of coprecipitated samples. The characteristic LDH diffraction lines disappeared completely at ca. 350 °C and a gradual crystallization of NiO-like mixed oxide was observed at higher temperatures. Hydrothermal treatment improved thermal stability of the Ni2Al and Ni3Al LDHs but only a slight effect of hydrothermal treatment was observed with the Ni4Al sample. The Rietveld refinement of powder XRD patterns of calcination products obtained at 450 °C showed a formation of Al-containing NiO-like oxide and a presence of a considerable amount of Al-rich amorphous component. Hydrothermal aging of the LDHs resulted in decreasing content of the amorphous component and enhanced substitution of Al cations into NiO-like structure. The hydrothermally treated samples also exhibited a worse reducibility of Ni^{2+} components. The $NiAl_2O_4$ spinel and NiO still containing a marked part of Al in the cationic sublattice were detected in the samples calcined at 900 °C. The Ni2Al LDHs hydrothermally treated for various times and related mixed oxides obtained at 450 °C showed an increase in pore size with increasing time of hydrothermal aging. The hydrothermal treatment of LDH precursor considerably improved the catalytic activity of Ni2Al mixed oxides in N_2O decomposition, which can be explained by suppressing internal diffusion effect in catalysts grains.

1. Introduction

Layered double hydroxides (LDHs), which are also known as hydrotalcite-like compounds or anionic clays, represent a class of layered materials with chemical composition expressed by the general formula $[M^{II}_{1-x}M^{III}_x(OH)_2]^{x+}[A^{n-}_{x/n}\cdot yH_2O]^{x-}$ where M^{II} and M^{III} are divalent and trivalent metal cations, A^{n-} is an n-valent anion and x has usually values between 0.20 and 0.33. The M^{II}/M^{III} isomorphous substitution in octahedral sites of the hydroxide sheets results in a net positive charge, which is neutralized by the interlayers composed of anions and water molecules. LDHs are often used in heterogeneous catalysis as precursors for preparation of mixed oxide catalysts [1–3]. After thermal decomposition at moderate temperatures, LDHs give finely dispersed mixed oxides of M^{II} and M^{III} metals with large surface area and good thermal stability. Calcined Ni–Al LDHs are used as catalysts of various reactions, for example in the steam reforming of methanol [4] or selective reduction of aldehydes to alcohols [5], and exhibit also a high activity in N_2O decomposition [6]. Thermal decomposition of LDHs was studied by many authors, a great number of studies were performed namely with synthetic Mg–Al hydrotalcite [7–9]. Two characteristic processes accompanied by a considerable weight loss and an endothermic effect can be observed during hydrotalcite heating: The release of interlayer water at 150–200 °C accompanied by a collapse of the LDH basal spacing [9,10] and the complete decomposition of the layered structure at 350–600 °C. The resulting structurally disordered oxide mixture crystallizes to form MgO-like phase above 400 °C; MgO and $MgAl_2O_4$ spinel are detected above 900 °C. The Ni–Al LDHs exhibit very similar thermal behavior with

* Corresponding author. Fax: +420 2 2431 1082.
E-mail address: Frantisek.Kovanda@vscht.cz (F. Kovanda).

0022-4596/$ - see front matter © 2008 Elsevier Inc. All rights reserved.
doi:10.1016/j.jssc.2008.09.014

thermal decomposition between 300 and 400 °C followed by crystallization of NiO (bunsenite). The $NiAl_2O_4$ spinel together with NiO is found by XRD in samples calcined at temperatures 900 °C and higher [11]. The formation of oxide phases during heating of Ni–Al LDHs was examined also using FTIR spectroscopy [12,13].

LDHs are usually prepared by coprecipitation, when a solution containing M^{II} and M^{III} metal cations in adequate proportions reacts with an alkaline solution. The product crystallinity can be affected by various reaction parameters (pH, temperature, concentration and flow rate of added solutions, and hydrodynamic conditions in the reactor) and/or post-synthesis operations (e.g., aging of the precipitate). A substantial improvement of the product crystallinity can be achieved by hydrothermal treatment at temperatures, which do not exceed the decomposition temperature of the LDHs. The hydrothermal crystallization is usually carried out at temperatures up to ca. 200 °C under autogenous pressure for a time ranging from hours to days. Some aspects of the hydrothermal treatment of hydrotalcite-like compounds at high temperatures have been discussed in the comprehensive article by Cavani et al. [1]. During hydrothermal treatment of Mg–Al hydrotalcite, the maximum crystallite size was achieved after long-time crystallization at 150–200 °C [14–18]. The hydrothermal treatment was also applied in order to improve the crystallinity of some LDHs containing nickel: Ni–Al [11], Ni–Al and Ni–Cr [19], Ni–Al–Cr and Ni–Al–Fe [20], and Ni–Fe [21]. Hydrothermal treatment of Ni–Al LDHs using microwave heating was also reported [22,23]. Well-crystallized products with a narrow distribution of particle size can be obtained during homogeneous precipitation in the presence of urea [24]. Recently, the microwave-assisted preparation of Ni–Al LDHs by urea hydrolysis [25] and reconstruction of calcined products in aqueous media [26] were reported. An alternative route for obtaining Ni–Al LDHs in the form of thin films is electrosynthesis using cathodic reduction of Ni and Al nitrates [27].

The layered crystal structure of hydrotalcite-like compounds collapses during thermal decomposition and the formed oxides are poorly crystalline with some amorphous portion gradually disappearing on further heating [28]. A relation between the precursor crystallinity and properties of the obtained mixed oxides can be expected. In the present work, the effect of hydrothermal treatment on physical chemical properties of both LDH precursor and related mixed oxides is studied. Thermal stability of the Ni–Al LDHs, changes in phase composition of the samples during heating, and structural and textural properties of the LDHs and related mixed oxides are examined. An effect of the precursor hydrothermal treatment on catalytic properties of the related mixed oxides is also explored, using catalytic N_2O decomposition as a testing reaction.

2. Experimental

2.1. Preparation of samples

The Ni–Al LDHs were prepared by coprecipitation. An aqueous solution (450 ml) of Ni and Al nitrates with Ni/Al molar ratio equal to 2, 3 or 4 and total metal ion concentration of 1.0 mol l^{-1} was added with flow rate of 80 ml min^{-1} into batch reactor containing 200 ml of distilled water. The flow rate of simultaneously added alkaline solution of 0.5 mol l^{-1} Na_2CO_3 and 3 mol l^{-1} NaOH was controlled to maintain the reaction pH of 10. The coprecipitation was carried out under vigorous stirring at 25 °C. The product was filtered off and a part of filtration cake was placed into 100 ml Teflon lined stainless steel bomb and resuspended in filtrate (mother liquor) to obtain 75 ml of suspension containing about 10 wt% of solid, which was hydrothermally treated at 180 °C for 20 h. After filtration, the product was washed thoroughly with distilled water and dried overnight at 60 °C. The remaining portion of the filtration cake was washed and dried without hydrothermal aging. The dried samples were heated for 4 h at 450 or 900 °C in air to obtain mixed oxides.

The prepared samples were denoted by acronyms with the molar ratios of the constituents and time of the hydrothermal treatment. For example, Ni2Al and Ni2Al-20 h denote the samples with Ni/Al molar ratio of 2 without hydrothermal aging and hydrothermally treated for 20 h, respectively. The calcined samples were denoted by analogous acronyms with the temperature value; for example, Ni2Al-20 h/450 denotes the Ni2Al-20 h sample calcined at 450 °C.

The system with Ni/Al molar ratio of 2 was studied in more details. The coprecipitated precursor was hydrothermally treated at 180 °C for 4, 8 and 20 h. The related mixed oxides prepared by LDH heating at 450 °C were crushed and sieved to obtain the fraction with particle size of 0.160–0.315 mm, which was used for surface area, porosity, TPR and catalytic measurements.

The reference NiO sample was prepared by calcination of β-$Ni(OH)_2$ at 450 °C for 4 h in air. The β-$Ni(OH)_2$ was synthesized by precipitation of an aqueous solution of nickel sulphate according to Yang [29].

2.2. Experimental techniques

Chemical composition of the prepared LDHs was determined by atomic absorption spectroscopy (AAS) using Perkin-Elmer 3100 instrument after sample dissolution in hydrochloric acid. Carbonate content was determined by analysis of CO_2 evolved during thermal decomposition of the sample using Eltra CS 500 instrument.

Thermal analyses, including thermogravimetry (TG), differential thermal analysis (DTA) and evolved gas analysis (EGA), were carried out using a Netzsch STA 409 instrument equipped by the quadrupole mass spectrometer QMS 403/4 (Balzers). The heating rate of 10 °C min^{-1}, air flow rate of 75 ml min^{-1} and 50 mg of sample were used. Gaseous products were continually monitored for chosen mass numbers m/z (18-H_2O^+ and 44-CO_2^+).

Powder X-ray diffraction patterns were recorded using a PANanalytical X'Pert PRO instrument with Co $K\alpha$ radiation ($\lambda = 0.179$ nm) in 2θ range 7–100°, step size 0.02°. The primary beam intensity was regularly checked between the measurements to make sure that the integral intensities of the diffraction lines are not affected by its variations; the variations were less than ±1%. The XRD measurements using silicon (SRM640c, NIST) as an internal standard were performed to evaluate the content of crystalline phases in mixed oxides obtained by calcination of Ni2Al LDH precursors at 450 and 900 °C. For refinement of lattice parameters and estimation of the mean coherence length (approximately equal to crystallite size), DiffracPlus Topas, release 2000 (Bruker AXS, Germany) was used. The structural models were taken from the Inorganic Crystal Structure Database ICSD, Retrieve 2.01 (FIZ Karlsruhe, Germany).

High-temperature powder XRD (HT XRD) measurements were performed in Anton Paar HTK16 high-temperature chamber with PANalytical X'Pert PRO diffractometer (Co $K\alpha$ radiation, X'Celerator multichannel detector) as described earlier [28]. The acquisition of XRD patterns at each temperature within several minutes was sufficiently fast to approach the dynamic conditions of TG/DTA/EGA measurements. To study the precursor decomposition and oxide phases crystallization, the scan in 2θ range 4–80° (Co $K\alpha$ radiation) with an effective heating rate of 0.85 °C min^{-1} between 25 and 400 °C (the step of 25 °C) was used. Then

the heating rate was raised to 3.3 °C min^{-1} between 400 and 900 °C (the step of 100 °C). HT XRD measurements were used to identify LDH decomposition temperatures.

TEM images were obtained using Transmission Electron Microscope Philips EM 201 at accelerating voltage of 80 kV and magnification of 130,000.

Surface area and mesoporous structure of the samples was determined by adsorption/desorption of nitrogen at 77 K using Micromeritics ASAP 2010 instrument. The total porous structure was characterized by Micromeritics AutoPore 9600 instrument working in the range 0.1–400 MPa.

The temperature-programmed reduction (TPR) measurements were carried out with 50 mg sample weight in a hydrogen–nitrogen mixture (10 mol% H_2) using flow rate of 50 ml min^{-1}. The temperature was linearly raised at the rate of 20 °C min^{-1} up to 800 °C. After freezing of rising water at −76 °C, a composition of gases was analyzed by thermal-conductivity detector.

The XPS spectra were measured by an ESCA 310 (Gammadata Scienta, Sweden) electron spectrometer with a base pressure 1×10^{-8} Pa. Samples were excited with Al $K\alpha$ radiation. The total energy resolution of the instrument was 0.65 eV as measured by FWHM of the Au $4f_{7/2}$ photoelectron peak. The powdered samples were deposited on the surface of gold plate and spectra were measured at room temperature and a pressure of 6×10^{-8} Pa. The following photoelectrons were recorded: Ni 2*p*, Ni 3*p*, Al 2*p*, Al 2*s* and O 1*s*. From all spectra a Shirley base was subtracted with a help of Gaussian–Lorentzian curve. In order to obtain information about the structure of the surface and the dispersion of the active phases, the surface atomic ratios were calculated as the ratio of the corresponding peak intensities, corrected with theoretical sensitivity factors based on Scofield's photoionization cross-sections [30].

The N_2O decomposition reaction was performed in a fixed-bed reactor of 5 mm internal diameter in temperature range from 330 to 450 °C with total flow rate of 100 ml min^{-1} NTP (273 K, 101.325 kPa), 0.1 g catalyst and 1000 ppm N_2O balanced by He. Before each run, the catalysts were pre-treated by heating in the He flow (50 ml min^{-1}, the heating rate 10 °C min^{-1}) up to 450 °C and maintaining the temperature for 1 h. Then the catalysts were cooled to reaction temperature and the steady state of N_2O at the reactor output was measured. The gas chromatograph Agilent Technologies 6890N equipped by TCD detector was used to determine N_2O concentration in the reactor inlet and outlet.

3. Results and discussion

3.1. Characterization of the Ni–Al LDH precursors

The results of chemical analysis of the coprecipitated and hydrothermally treated Ni–Al LDHs are summarized in Table 1 and the structural characteristics of the LDHs evaluated from the XRD data are presented in Table 2. The Ni/Al molar ratio in products dried at 60 °C corresponded approximately to those in the nitrate solution used for coprecipitation. The hydrothermal treatment did not influence the content of Ni and Al cations in the LDH. Slightly increased content of carbonate was found in the coprecipitated samples without hydrothermal aging. A trace amount of residual sodium cations (<0.03 wt%) remained in the washed and dried samples. In the powder XRD patterns of the dried samples without hydrothermal treatment, only a hydrotalcite-like phase exhibiting relatively low crystallinity was detected. The crystalline hydrotalcite-like phase was formed in spite of the application of relatively rapid flow rate of nitrate solution (80 ml min^{-1} instead of the conventional dropwise addition). The hydrothermal treatment resulted in an increasing

Table 1
Chemical composition of the coprecipitated and hydrothermally treated LDHs

Sample	(wt%)				Ni/Al molar ratio
	Ni	Al	Na	CO_3^{2-}	
Ni2Al	35.4	8.40	0.019	10.65	1.94
Ni2Al-4 h	35.6	8.60	0.029	9.70	1.90
Ni2Al-8 h	35.4	8.40	0.016	9.52	1.94
Ni2Al-20 h	35.8	8.40	0.021	9.63	1.96
Ni3Al	38.0	5.80	0.004	9.27	3.01
Ni3Al-20 h	40.2	6.40	0.019	8.15	2.89
Ni4Al	40.6	4.56	0.002	8.85	4.09
Ni4Al-20 h	41.6	4.66	0.012	7.98	4.10

Table 2
Results of XRD analysis of the coprecipitated and hydrothermally treated LDHs

Sample	(003) integral intensity	(003) FWHM	Crystallite size[a]	Lattice parameter (Å)	
	(a.u.)	(°2θ)	(nm)	*a*	*c*
Ni2Al	17,428	2.29	4.1	3.022	22.73
Ni2Al-4 h	23,666	0.66	14.0	3.026	22.70
Ni2Al-8 h	24,167	0.55	16.9	3.027	22.70
Ni2Al-20 h	24,859	0.37	25.2	3.027	22.71
Ni3Al	16,253	2.19	4.2	3.042	23.44
Ni3Al-20 h	66,260	0.36	25.8	3.042	23.09
Ni4Al	17,473	2.02	4.6	3.050	23.57
Ni4Al-20 h	19,232	1.23	7.5	3.055	23.54

[a] Crystallite size calculated as XRD coherent domain in [001] direction using Scherrer's formula.

intensity of the hydrotalcite diffraction lines (Fig. 1). A trace amount of AlOOH (boehmite) was detected in the powder XRD pattern of the Ni2Al-20 h sample. From XRD data processing, the (003) diffraction line integral intensity, FWHM value, crystallite size in [001] direction and lattice parameters of the prepared LDHs were evaluated (Table 2).

Powder XRD patterns of the Ni2Al samples showed that the FWHM value of (003) diffraction line decreased with increasing time of hydrothermal treatment, which indicated an increase of the LDH crystallite size. A marked increase of the LDH crystallite size (calculated as a mean coherence length using Scherrer's formula) was observed already after a relatively short time of hydrothermal treatment (4 h) and the prolonged aging time resulted in a further ordering of the LDH crystal structure. The increasing time of hydrothermal treatment resulted also in an increase of the integral intensity of LDH (003) diffraction line, which can indicate rising content of the crystalline LDH phase in the samples. In dependence on aging time, a marked increase in the (003) line integral intensity was observed especially between the hydrothermally treated Ni2Al samples and the non-treated one. The maximum difference in the (003) line integral intensity was observed between the Ni3Al and Ni3Al-20 h samples but the corresponding FWHM values were comparable to those evaluated for Ni2Al and Ni2Al-20 h samples, respectively. On the other hand, only a minimum effect of the hydrothermal aging was observed for the Ni4Al sample with high Ni/Al molar ratio. The lattice parameters were not changed during LDH hydrothermal treatment. Only an insignificant increase in lattice parameter *a*, and decrease in lattice parameter *c* between hydrothermally aged samples and non-treated ones was found (Table 2). Benito et al. [23] reported on similar changes in lattice parameter *c* and

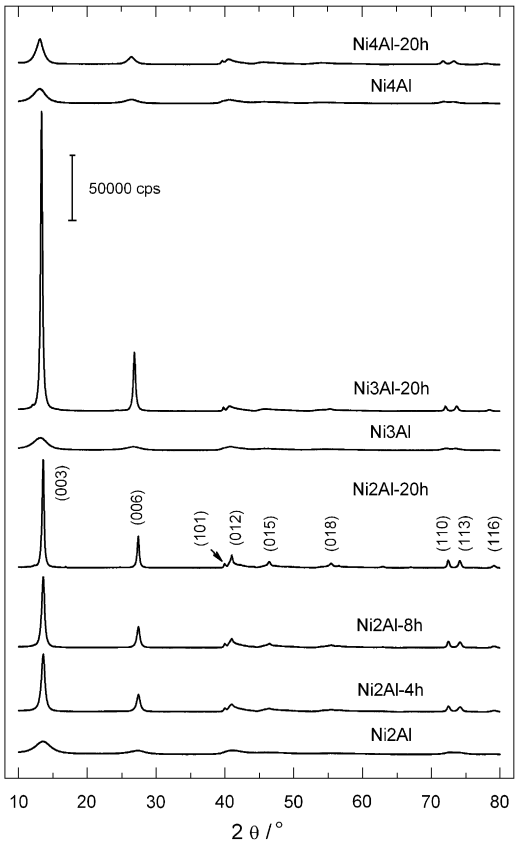

Fig. 1. Powder XRD patterns of the coprecipitated and hydrothermally treated Ni–Al LDHs.

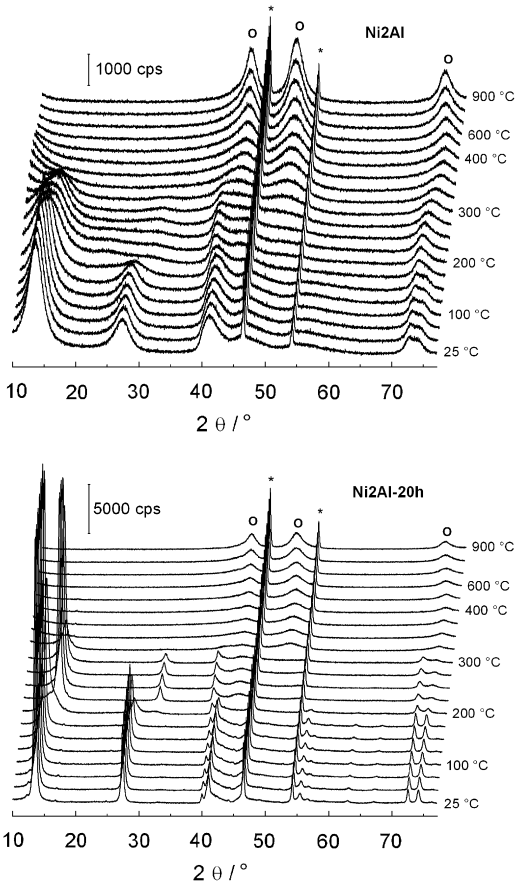

Fig. 2. HT XRD patterns of the non-treated Ni2Al and hydrothermally treated Ni2Al-20 h samples. O—Ni–Al mixed oxide, *—Pt support.

assigned them to strengthening interaction between interlayer anions and hydroxide layers.

3.2. Thermal decomposition

Thermal decomposition of the prepared Ni–Al LDHs was studied using conventional thermal analysis and HT XRD as in [28]. During HT XRD measurements, powder XRD patterns with the temperature step of 25 °C were obtained between 25 and 400 °C. In general, two essential stages can be observed during phase transformation of LDHs upon heating: (i) a shift of LDH basal spacing associated with release of interlayer water and (ii) disappearing of the LDH diffraction lines and formation of oxide phases. Stanimirova et al. [10] discussed the mechanism of LDH collapse; the collapsed phase retaining the layered structure of the pristine LDH was denoted as metahydrotalcite B. An analogous phase observed during heating of cobalt-containing LDHs we denoted as collapsed LDH; it had basal spacing decreased typically from about 7.6 to 6.6 Å [28]. Similar shift of the basal spacing was found also for the examined Ni-Al LDHs.

The basal spacing d_{003} of about 7.55 Å was evaluated for the dried Ni2Al sample. During HT XRD measurement, the basal spacing was not changed up to 150 °C and then it was slightly shifted to about 7.35 Å. Between 250–300 °C, a marked shift to about 6.85 Å was observed and the LDH basal diffraction lines disappeared at 350 °C. Hydrothermally treated samples (Ni2Al-4 h, Ni2Al-8 h and Ni2Al-20 h) exhibited very similar changes in basal spacing in dependence on heating temperature: At lower temperatures (25–175 °C) the same basal spacing of 7.55 Å was evaluated. At 200 °C, slightly shifted basal diffraction lines (003) and (006) with lower intensity were observed and collapsed LDH phase with basal spacing of 6.6 Å was found between 225 and 300 °C. Further heating of the samples resulted in decreasing intensity of the LDH diffraction lines, which disappeared completely at 350 °C. The HT XRD patterns of the Ni2Al and Ni2Al-20 h samples are shown in Fig. 2.

The results of thermal analysis of the Ni2Al samples hydrothermally treated for various times are demonstrated in Fig. 3. Two major endothermic effects, characteristic for hydrotalcite-like compounds, were observed in DTA curves. The first one was associated with H_2O evolution and corresponded to a release of interlayer water. It was observed at 240 °C for the Ni2Al sample and at 275–280 °C for the hydrothermally treated ones. The second endothermic effect was accompanied by simultaneous H_2O and CO_2 evolution associated with dehydroxylation of hydroxide layers and decomposition of interlayer carbonate. Both thermal analysis and HT XRD measurements showed that hydrothermal aging enhanced thermal stability of the coprecipitated LDHs (Table 3).

The Ni3Al and Ni4Al samples exhibited an analogous thermal behavior like Ni2Al one before and after hydrothermal aging. The basal spacing of about 7.8 Å evaluated for the Ni3Al sample gradually decreased between 100 and 175 °C to achieve ca. 6.8 Å. The collapsed LDH with basal spacing of about 6.7 Å was detected at 200–300 °C and this phase disappeared at 325 °C. The hydrothermally treated Ni3Al sample exhibited basal spacing of 7.7 Å. A marked shift of the basal spacing to 6.6 Å was observed between 175 and 200 °C. The collapsed phase was stable at 200–300 °C and disappeared completely at 350 °C (a residual (003) diffraction peak of the collapsed phase was detected up to 325 °C). A dehydration of the interlayer space during heating of the Ni–Al LDH with Ni/Al molar ratio of 3 was recently discussed

by Pérez-Ramírez et al. [31]. A continuous decrease of the interlayer space was observed in the temperature range of 150–200 °C. Contrarily to the Mg–Al LDH, the rehydration of dehydrated Ni–Al sample was not fully reversible and no reconstruction of the Ni–Al mixed oxide prepared by LDH calcination at 450 °C was observed.

A gradual shift of the basal spacing from about 7.85 to 6.6 Å in the temperature range 100–150 °C was observed also with the Ni4Al sample. The collapsed phase with d_{003} of 6.55 Å was detected at 200–275 °C and it disappeared at 300–325 °C. The hydrothermal aging of the Ni4Al sample did not affect significantly its thermal behavior. Between 125 and 175 °C the Ni4Al-20 h sample with basal spacing of 7.85 Å was gradually converted to the collapsed LDH with d_{003} of about 6.7 Å, which disappeared completely at 325–350 °C. The phase changes detected by HT XRD were observed at lower temperatures than that corresponding DTA effects and gases evolution maxima measured during thermal analysis. This event can be explained by a difference in the used heating rates. On the other hand, similar disagreement between HT XRD and thermal analysis results was observed with cobalt-containing LDHs [28], when the same heating rates were used. It can be expected that maximum evolution of gases (and corresponding DTA effect) takes place after at least partial destruction of the ordered LDH crystal structure and that the gaseous products are evolved from already partly amorphous intermediate.

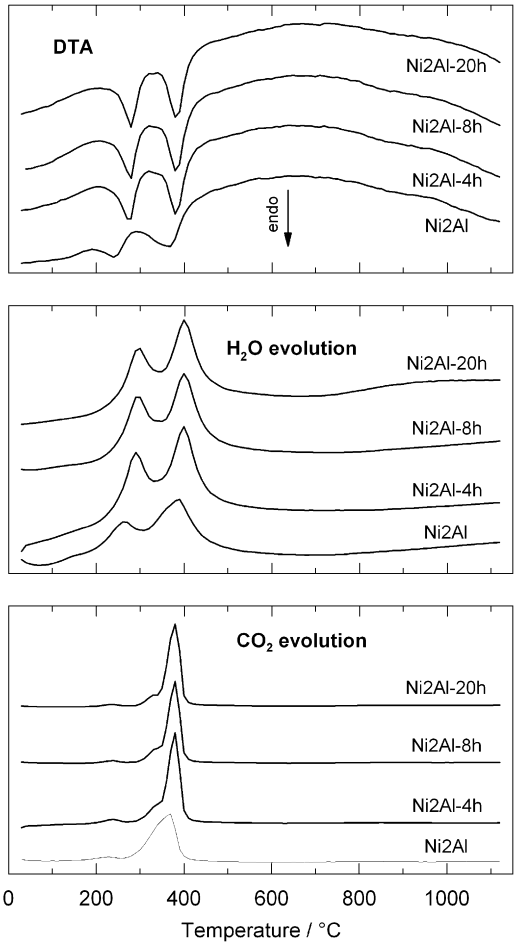

Fig. 3. Results of thermal analysis of the Ni2Al samples hydrothermally treated for various times.

TEM images (Fig. 4) showed a marked increase of the LDH crystal size during hydrothermal treatment. The aggregates composed of small thin crystals with hexagonal morphology were observed in the coprecipitated samples. The product aging under hydrothermal conditions increased the crystal size to achieve hexagonal platelets with diameter of nearly 100 nm after 20 h treatment. The size and hexagonal morphology of the primary LDH crystals was kept even after their thermal decomposition at 450 °C, when Ni–Al mixed oxide was formed. However, the integrity of initially compact hexagonal platelets was slightly affected by narrow pores formed likely due to a release of volatile components (H_2O and CO_2) during LDH heating. A partial destruction of the hexagonal platelets can be seen in the TEM images of the samples calcined at 900 °C. It can be explained by recrystallization processes and formation of other oxide phases at high calcination temperatures.

3.3. Formation of the mixed oxides

HT XRD measurements showed that characteristic LDH diffraction lines disappeared around 350 °C in all examined samples and rather amorphous calcination products are formed. A gradual crystallization of NiO-like mixed oxide with increasing temperature can be seen in Fig. 2. Ambient XRD measurements showed starting crystallization of NiO (bunsenite) at ca. 400 °C [11,32]. Increasing calcination temperature enhanced the crystallization of NiO-like phase and additionally $NiAl_2O_4$ spinel was detected in the samples calcined at 800–900 °C and higher temperatures.

The powder XRD patterns of the mixed oxides obtained by heating of Ni2Al samples at 450 and 900 °C (Fig. 5) were evaluated in more details to examine an influence of the LDH precursor hydrothermal treatment on phase composition of the calcination products. The lattice parameter of the NiO-like phase formed at 450 °C was slightly lower in comparison with reference NiO

Table 3
Thermal decomposition characteristics of coprecipitated and hydrothermally treated LDHs obtained by thermal analysis (temperatures of DTG minima, DTA minima and maximum H_2O and CO_2 evolution) and high-temperature X-ray diffraction

Sample	T of Δm minima (DTG) (°C)	T of ΔT minima (DTA) (°C)	-H_2O (EGA) (°C)	-CO_2 (EGA) (°C)	LDH dehydration (HT XRD) (°C)	LDH destruction (HT XRD) (°C)
Ni2Al	232; 356	240; 365	265; 389	368	200	350
Ni2Al-4 h	265; 370	275; 378	290; 400	380	225	350
Ni2Al-8 h	270; 370	280; 381	296; 400	379	225	350
Ni2Al-20 h	269; 371	280; 380	297; 400	380	225	350
Ni3Al	(135, 189); 331	145; 340	207; 340	340	175	325
Ni3Al-20 h	240; 349	248; 351	250; 350	357	200	350
Ni4Al	147; 318	158; 330	162; 330	330	150	300
Ni4Al-20 h	182; 326	180; 330	221; 331	333	150	325

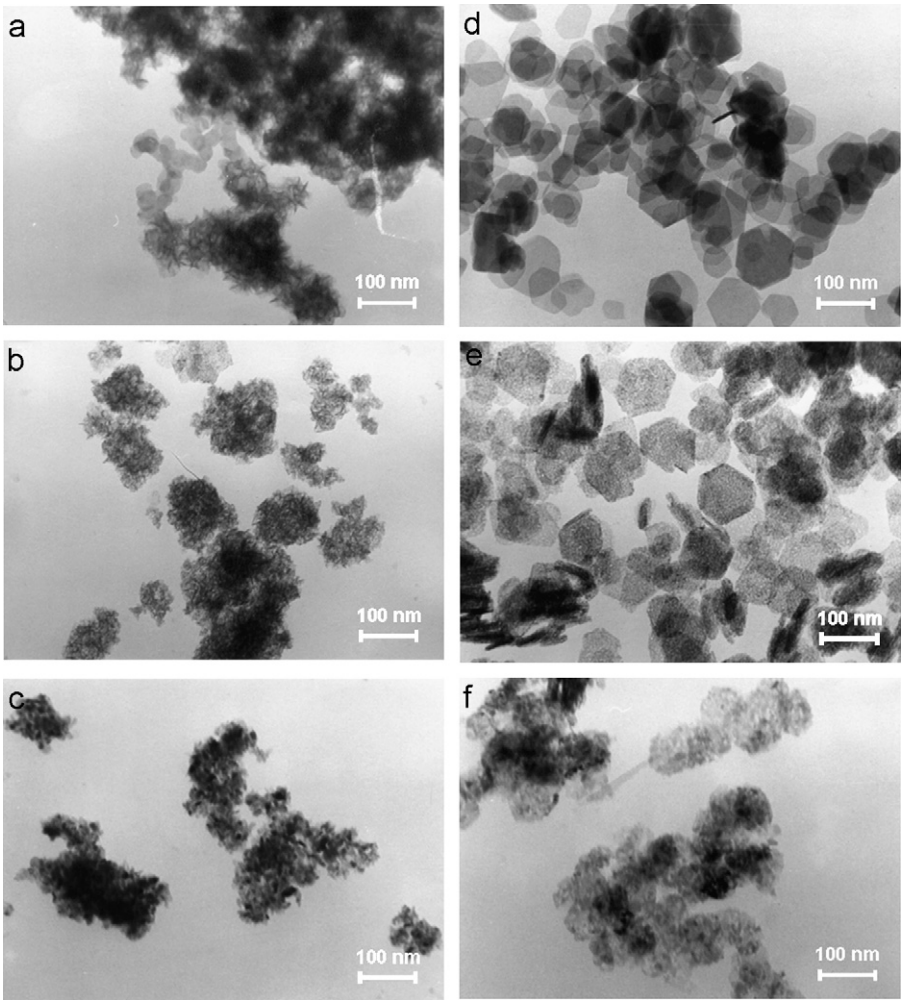

Fig. 4. TEM images of the non-treated Ni2Al and hydrothermally treated Ni2Al-20 h samples and related mixed oxides obtained at 450 and 900 °C. a—Ni2Al, b—Ni2Al/450, c—Ni2Al/900, d—Ni2Al-20 h, e—Ni2Al-20 h/450, f—Ni2Al-20 h/900.

(Table 4). No separate Al-containing phase was observed by XRD that could mean either a segregation of Al cations to an amorphous components or their incorporation into the NiO-like phase or both. The Al incorporation into NiO lattice seems to be in line with decreasing the NiO lattice parameter on decreasing Ni/Al molar ratio in the samples. It is obvious that the lattice shrinkage is larger in oxides formed from hydrothermally aged LDHs; the aging also resulted in larger crystallite size of the calcined products (Table 4) and lower content of amorphous components (Table 5). The content of the amorphous components is approximately equal (non-treated sample) or lower (hydrothermally treated ones) compared to the total content of Al_2O_3 in the system (25.44 wt% for mixed oxide with Ni/Al molar ratio of 2). The amorphous components were not found in the samples calcined at 900 °C but the content of $NiAl_2O_4$ spinel is still lower than it would correspond to a portion of aluminum available in the formed oxide mixture: if all aluminum was included in the $NiAl_2O_4$ spinel, its content would be equal to 44.08 wt%. The results of Rietveld refinement can be explained by formation of a mixture of Al-rich amorphous component and Al-containing NiO-like oxide at 450 °C, followed by recrystallization at 900 °C to $NiAl_2O_4$ spinel and NiO still containing of about 20 mol% Al in the cationic sublattice. Trifiro et al. [33] reported a substantial dissolution of Al^{3+} ions during treatment of calcined Ni–Al LDHs in a NaOH solution; this event was explained by presence of an alumina-type phase, probably grafted on the spinel-type phase. However, this is not the case in phases here reported, because XPS analysis did not indicate a surface enrichment by Al in relation to the bulk (see below). With respect to stoichiometric NiO both evaluated contents of components and decrease in the lattice parameter of NiO-like phase in the calcination products (900 °C) indicate a rather enhanced incorporation of Al cations into the NiO lattice in hydrothermally treated samples.

3.4. Porous structure

The physical chemical properties of the Ni2Al LDHs hydrothermally treated for various times and related mixed oxides obtained at 450 °C were studied in more details because these mixed oxides were also tested in the catalytic decomposition of N_2O. The BET surface area of the dried LDHs increased after short-time hydrothermal treatment (from 70 to 87 $m^2 g^{-1}$ measured for Ni2Al and Ni2Al-4 h samples, respectively). Long-time hydrothermal treatment decreased significantly the LDH surface area (52 $m^2 g^{-1}$ measured for Ni2Al-20 h sample), which can be explained by dissolution and recrystallization of the smallest crystallites and amorphous particles and subsequent increase of the LDH crystallite size during hydrothermal aging. The growth of LDH crystals during hydrothermal aging was confirmed by XRD and TEM results. The calculated volumes of micropores with diameter lower than 2 nm (Table 6) showed that all LDH samples have very low volume of micropores and evaluated surface area can be ascribed to mesopores. Pore size distribution was evaluated

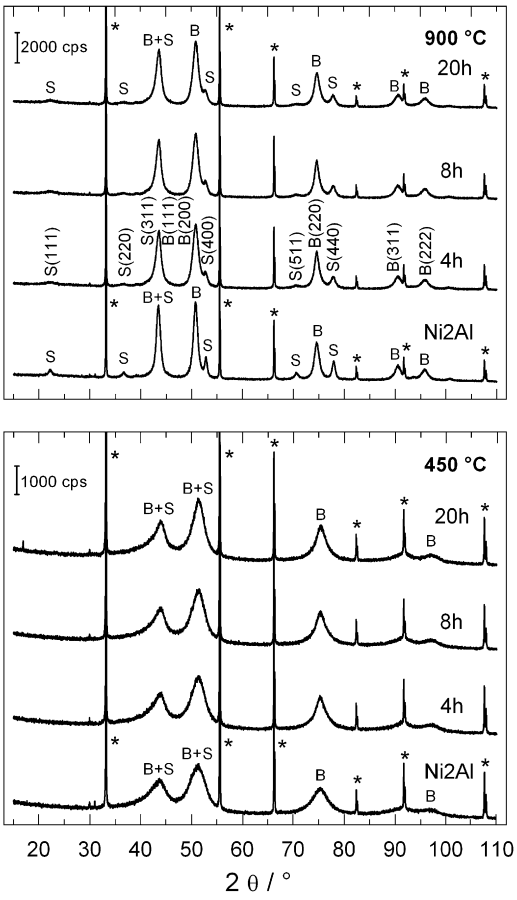

Fig. 5. Powder XRD patterns of the Ni2Al samples hydrothermally treated for various times and calcined at 450 and 900 °C. B—NiO (bunsenite), S—$NiAl_2O_4$ (spinel), *—Si (internal standard).

Table 4
Lattice parameter and crystallite size of NiO-like mixed oxide obtained by calcination of the LDHs at 450 °C

Sample	Lattice parameter (Å)	Crystallite size[a] (nm)
Ni2Al/450	4.148	3.3
Ni2Al-4 h/450	4.138	3.9
Ni2Al-8 h/450	4.137	4.0
Ni2Al-20 h/450	4.138	5.0
Ni3Al/450	4.166	4.6
Ni3Al-20 h/450	4.158	4.9
Ni4Al/450	4.173	5.1
Ni4Al-20 h/450	4.170	4.8
NiO	4.177	n.d.

n.d.—Not determined.
[a] Crystallite size was obtained by Rietveld refinement (whole pattern fitting).

from nitrogen desorption isotherm measured at −196 °C. The Ni2Al sample exhibited a sharp maximum corresponding to the pore radius of 1.9 nm and then a low and broad maximum at r_{max} of about 11 nm. Hydrothermal aging of the LDH precursor resulted in a marked increase of the pore size, which increased with time of hydrothermal treatment (Table 6).

Total intrusion pore volume increased with time of hydrothermal treatment and increased from 0.31 to 0.65 $cm^3\,g^{-1}$ measured for Ni2Al and Ni2Al-20 h samples, respectively. Bulk density is inversely connected with the total pore volume and decreased with increasing time of hydrothermal treatment. Helium density of the LDH samples was not affected significantly by hydrothermal aging and corresponded approximately to 2.62–2.66 $g\,cm^{-3}$. The increasing porosity of the LDHs can be explained by growth of the crystallites during hydrothermal treatment. For Ni2Al sample, the mercury intrusion showed much wider pores (r_{max} of 10 and 24 nm) in comparison with nitrogen desorption (r_{max} of 1.9 nm). On the other hand, pores with only slightly lower size were found in hydrothermally treated LDHs. In all measured samples, no pores with r_{max} higher than 100 nm were detected (Fig. 6).

The BET surface area of the calcination products increased more than two times in comparison with the LDH precursors and slightly increased with time of LDH hydrothermal aging. The volume of micropores was also increased but it remained negligible in relation to the total pore volume as evaluated surface area corresponded to mesopores. Larger pore volume resulted in lower bulk density and higher porosity of the calcined samples. Helium density of the obtained mixed oxides slightly increased with the time of LDH hydrothermal treatment from 4.02 to 4.26 evaluated for Ni2Al/450 and Ni2Al-20 h/450 samples, respectively. Pores with r_{max} of 2.5 nm were detected in the Ni2Al/450 sample by nitrogen desorption. Slightly wider pores in comparison with the parent LDHs were found also for the hydrothermally treated samples (Table 6) but a minor part of the pores detected in these samples exhibited r_{max} of about 1.7 nm. Formation of such narrow pores could be connected with release of the volatile components during thermal decomposition of the LDH precursors.

3.5. TPR results

The TPR patterns of the Ni2Al samples calcined at 450 °C are demonstrated in Fig. 7. They exhibit broad reduction peak with maximum in the temperature range 523–614 °C, which corresponds to reduction of $Ni^{2+} \rightarrow Ni^0$; the reducibility of the samples worsened with increasing time of hydrothermal treatment. The reduction maxima of the calcined Ni2Al samples were observed at much higher temperatures than the reduction maximum of the reference NiO (330 °C). A formation of small and stable NiO particles can be expected during calcination of Ni2Al LDH precursors at 450 °C; however, they are worse reducible in

Table 5
Results of Rietveld refinement of oxide phases formed by heating Ni2Al LDHs hydrothermally treated for various times (content of amorphous components was obtained using addition of known amount of Si internal standard)

LDH precursor	450 °C		900 °C			
	NiO (wt%)	Amorphous (wt%)	NiO (wt%)	NiO lattice parameter (Å)	Spinel (wt%)	Spinel lattice parameter (Å)
Ni2Al	74.6	25.4	62.1	4.177	37.9	8.052
Ni2Al-4 h	78.8	21.2	64.8	4.176	35.2	8.065
Ni2Al-8 h	82.0	18.0	64.9	4.176	35.1	8.067
Ni2Al-20 h	77.7	22.3	64.9	4.174	35.1	8.068

Note: No amorphous components were found in the samples calcined at 900 °C.

Table 6
Surface area and the porous structure of the hydrothermally treated Ni2Al LDH precursors and related mixed oxides obtained by calcination at 450 °C

Sample	Nitrogen adsorption				Mercury intrusion			
	Surface area (S_{BET}) ($m^2 g^{-1}$)	Pore volume ($cm^3 g^{-1}$)	Volume of micropores ($mm^3 g^{-1}$)	Pore size (r_{max}) (nm)	Total pore volume ($cm^3 g^{-1}$)	Bulk density ($g cm^{-3}$)	Porosity (%)	Pore size (r_{max}) (nm)
Ni2Al	70	0.19	0.9	1.9	0.31	1.51	46.5	10; 24
Ni2Al-4 h	87	0.34	2.1	9.5	0.44	1.24	54.8	6
Ni2Al-8 h	74	0.33	1.1	13	0.51	1.17	59.9	9
Ni2Al-20 h	52	0.19	0.7	17	0.65	0.98	63.6	17; (28)
Ni2Al/450	145	0.40	3.2	2.7	0.48	1.34	64.6	2.8; (11); 18
Ni2Al-4 h/450	144	0.60	3.5	(1.7); 12	0.67	1.06	70.9	7.5; (12)
Ni2Al-8 h/450	154	0.75	5.5	(1.7); 16	0.74	1.08	80.2	10; (18)
Ni2Al-20 h/450	161	0.75	2.5	(1.7); (12); 28	0.92	0.85	77.9	17

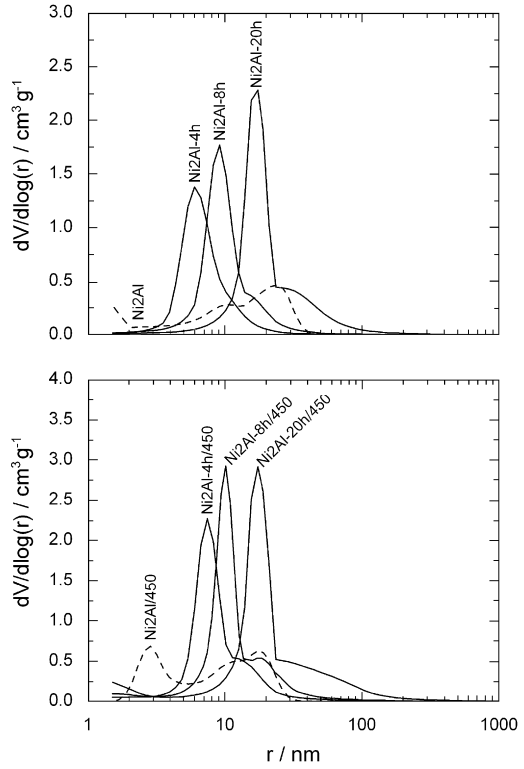

Fig. 6. Pore size distribution of the Ni2Al samples hydrothermally treated for various times and related mixed oxides obtained at 450 °C (mercury intrusion porosimetry).

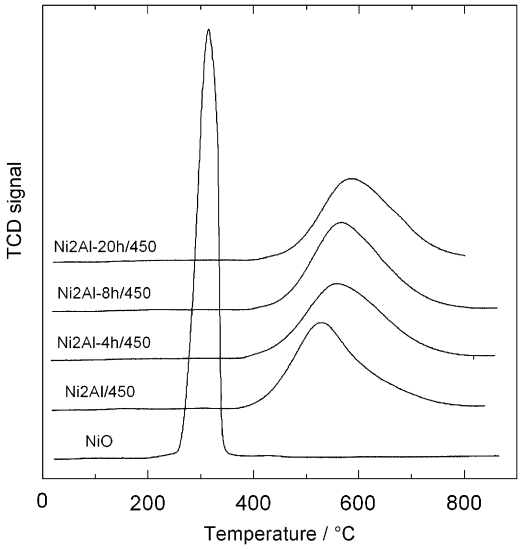

Fig. 7. TPR patterns of hydrothermally treated Ni2Al samples calcined at 450 °C.

comparison with stoichiometric NiO. It is known that reduction of Ni–Al LDH-related mixed oxides is hindered by the presence of nickel aluminate-type phases formed likely upon heating of the LDH precursor [11,23,33].

Data obtained from TPR measurements are summarized in Table 7. Only a slight difference was observed in amount of hydrogen consumed for total reduction of all examined samples, the lowest amount of reducible components being detected in the sample without hydrothermal treatment. Two individual peaks were distinguished by fitting the total reduction peak. These two peaks are associated with two different arrangement of the primary particles or occurrence of two different phases in the samples. Positions of both peaks maxima shifted to higher temperatures and the amount of easily reducible components (corresponding to the first reduction peak) decreased with increasing time of hydrothermal treatment. The better structural ordering and increased crystallite size of hydrothermally treated Ni2Al LDH precursors enhanced the stability of Ni^{2+} species in calcination products against reduction as it was formerly reported [23]. Worsened reducibility of the calcination products prepared from hydrothermally aged LDH precursors could be also caused by an enhanced incorporation of the Al cations into the NiO lattice as it was deduced from the results of Rietveld refinement.

3.6. Surface composition

The XPS spectra of Ni2Al samples calcined at 450 °C were collected and compared with reference NiO. The samples were deposited on a gold support and examined in the powdered form. The reference NiO and the Ni2Al-8 h/450 sample were additionally examined after 30 min heating at 400 °C to identify the form of surface oxygen in the samples. Oxidation state of nickel on the surface was determined from binding energy and its chemical shift in the XPS spectra (Table 8). According to the published data determined by examination of oxides, hydroxides and oxohydroxides [34], the binding energies of Ni $2p_{3/2}$ for oxidation state Ni^0, Ni^{2+}, and Ni^{3+} are equal to 852.8, 854.6 and 856.1 eV, respectively. Electron structure and theoretical models of pure Ni and NiO are discussed in [34–36]. Interpretation of the Ni 2*p* spectra of oxides and other compounds is based on the transfer of charge of both the main peak at 854.6 eV and the wide satellite with binding

Table 7
TPR results of the Ni2Al samples hydrothermally treated for various times and calcined at 450 °C

Sample	H_2 consumption (20–800 °C) (mmol H_2 g^{-1})	T_{max}[a] (°C)	Peak area[a] (%)	H_2 consumption[b] (mmol H_2 g^{-1})
Ni2Al/450	8.58	523; 585	44; 56	3.77
Ni2Al-4 h/450	8.68	561; 609	54; 46	4.69
Ni2Al-8 h/450	8.80	560; 602	36; 64	3.17
Ni2Al-20 h/450	8.82	570; 614	21; 79	1.85

[a] Determined from peak fitting.
[b] Hydrogen consumption corresponding to the first reduction peak.

Table 8
Binding energy of internal electrons and FWHM values of the photoemission peaks (in parenthesis)

Sample	Al $2p_{3/2}$	Ni $2p_{3/2}$		Ni $3p_{3/2}$	O 1*s*		
	Al^{3+}	Ni^{2+}	Satellite	Ni^{2+}	O^{2-}	O^{2-} OH^-	$H_2O_{ads.}$
NiO	–	855.5 (4.1)	861.5	67.9 (3.8)	530.0	531.7 (1.9)	
NiO/h[a]	–	855.1 (4.7)	861.1	68.2 (4.7)	530.0 (3.9)		
Ni2Al/450	73.6 (2.2)	855.7 (4.4)	861.7	67.9 (3.9)	530.0	531.7 (2.3)	533.0
Ni2Al-4 h/450	73.6 (2.2)	855.5 (4.2)	861.4	68 (4.3)	530.0	531.6 (2.3)	533.2
Ni2Al-8 h/450	73.5 (2.2)	855.7 (4.0)	861.5	68.1 (4.0)	530.0	531.6 (2.3)	533.1
Ni2Al-8 h/450/h[a]	73.6 (2.7)	855.4 (4.0)	861.5	68.2 (4.3)	530.0	531.7 (2.4)	
Ni2Al-20 h/450	73.6 (2.2)	855.5 (3.9)	861.6	68.1 (4.0)	530.0	531.6 (2.3)	533.2

Data are related to the O 1*s* line (binding energy of 530.0 ± 0.2 eV).
[a] Samples heated for 30 min at 400 °C before XPS measurement.

Table 9
Surface concentration of Ni and Al cations (C_S) and ratio of surface to bulk concentration (C_S/C_V)

Sample	C_S (mol.%)		C_S/C_V	
	Al^{3+}	Ni^{2+}	Al^{3+}	Ni^{2+}
NiO	0	1.00	0	1
NiO/h[a]	0	1.00	0	1
Ni2Al/450	0.33	0.67	1	1.02
Ni2Al-4 h/450	0.31	0.69	1	1.11
Ni2Al-8 h/450	0.34	0.66	1	0.97
Ni2Al-8 h/450/h[a]	0.33	0.67	1	1.02
Ni2Al-20 h/450	0.34	0.66	1	0.97

[a] Samples heated for 30 min at 400 °C before XPS measurement.

energy of 861 eV corresponding to cd^9L (c = vacancy in a nucleus, L = ligand vacancy) and naked cd^8 configurations.

Concentrations of the elements present on the samples surface were calculated from the Al 2*p*, Ni 2*p* and O 1*s* photoelectron lines. The C 1*s* photoelectron line was not measured, as carbon was not either present or only in a very low concentration in the examined samples. The electron spectra of O 1*s* consisted of three overlapping components, from which the component with the highest binding energy, i.e., the low intensive one likely belongs to adsorbed H_2O. This component disappeared in the XPS spectrum of the Ni2Al-8 h/450 sample after its heating at 400 °C, which confirmed this assumption. The surface concentrations of Ni and Al close to the bulk ones were found and only a very slight enrichment of mixed oxide surface with nickel could be expected (Table 9).

3.7. Catalytic activity in N_2O decomposition

Catalytic decomposition of nitrous oxide is a simple redox reaction, which was often chosen as a testing reaction for finding a correlation between structural and catalytic properties of solids [6]. The catalytic decomposition offers also a simple method for abatement of N_2O in waste gases. The temperature dependence of N_2O decomposition over Ni2Al samples calcined at 450 °C is shown in Fig. 8. It can be seen that hydrothermal treatment enhanced the catalytic activity of related mixed oxide catalysts; the Ni2Al-20 h/450 sample exhibited the highest N_2O conversion from all examined catalysts. Temperature T_{50}, at which 50% conversion of N_2O was observed, decreased with increasing time of hydrothermal treatment and the difference of T_{50} between the Ni2Al/450 and Ni2Al-20 h/450 samples was about 25 °C.

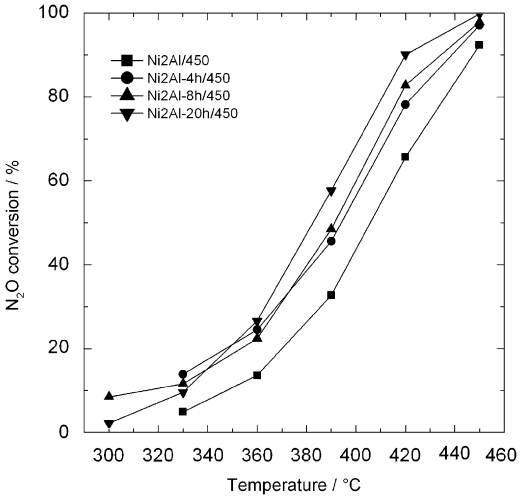

Fig. 8. Temperature dependences of N_2O conversion over hydrothermally treated Ni2Al samples calcined at 450 °C. (Conditions: 1000 ppm N_2O balanced by He, total flow 100 ml min^{-1}, catalyst weight 0.1 g)

The enhanced catalytic activity of hydrothermally treated samples could be related to a decreased amount of amorphous admixture (as it was observed by XRD). The surface area of the

calcined products was influenced only slightly by hydrothermal treatment of the LDH precursor. We have found [6] that the total surface area is not a crucial factor affecting the catalytic activity of Ni–Al mixed oxides in N_2O decomposition. Actually the pore size distribution in the examined samples changed in dependence on time of LDH hydrothermal aging (Fig. 6), and there is obviously a positive correlation between catalytic activity and porous structure. In such a case, the influence of the diffusion processes can be very likely considered.

Hence, we have estimated the Weisz–Prater criterion [37] to determine whether the internal diffusion in the pores is limiting the reaction rate. A negligible concentration difference in the catalyst grains can be expected for Weisz–Prater criterion $\ll 1$ and consequently no diffusion limitations occur at such conditions. On the other hand, the internal diffusion causes a decrease in the observed reaction rate for Weisz–Prater criterion $\gg 1$. Following parameters were chosen for calculation of the criterion values: Bulk density of the catalyst ranging from 600 to 1800 $kg\,m^{-3}$ and radius of the grains ranging from 0.8×10^{-4} to 1.6×10^{-4} m. The Weisz–Prater criterion, calculated within these limits, changed from 10.7 to 0.2 for Ni2Al/450 and Ni2Al-20 h/450 samples, respectively. Based on the calculated values of the Weisz–Prater criterion, the differences in catalytic activity of the examined Ni–Al mixed oxides can be explained by a decelerating effect of the internal diffusion in the catalysts grains.

4. Conclusions

Hydrothermal treatment of the coprecipitated Ni–Al LDHs improved significantly crystallinity of the samples. As it was observed with the Ni2Al samples, a marked difference was found especially between the hydrothermally treated samples and the non-treated one.

The dehydration of interlayer space of LDHs resulted in the shift of their basal spacing and formation of the collapsed layered phase. The characteristic LDH diffraction lines disappeared completely at approximately 350 °C and a gradual crystallization of NiO-like mixed oxide phase was observed at higher temperatures. Thermal stability of LDHs decreased with increasing Ni/Al molar ratio. Hydrothermal treatment improved thermal stability of the LDHs with Ni/Al molar ratio of 2 and 3 but only a slight effect of hydrothermal treatment was observed for the sample with Ni/Al molar ratio of 4.

The NiO-like Ni–Al mixed oxide was formed after LDH thermal decomposition. The hydrothermal treatment of LDH precursors resulted in decreasing content of amorphous component in calcined samples and enhanced incorporation of Al cations into NiO-like structure. The hydrothermally treated samples exhibited a worse reducibility of Ni^{2+} species in calcination products. Even after crystallization of $NiAl_2O_4$ spinel at high calcination temperature (900 °C), a marked part of Al cations remained in the NiO-like oxide.

An increase in pore size with increasing time of hydrothermal aging was observed in the Ni2Al LDHs. Heating of LDHs at 450 °C increased considerably the surface area and pore volume of the calcined samples and slightly increased also the size of pores. Both LDH precursors and calcined samples exhibited mesoporous structure with minimum volume of micropores. The pore size distribution in calcined samples likely influenced the activity of examined Ni–Al mixed oxides in catalytic decomposition of N_2O. A decelerating effect of the internal diffusion in the catalysts grains was suppressed by hydrothermal aging of the Ni2Al LDH and the efficiency of related mixed oxides in N_2O decomposition increased with increasing time of hydrothermal aging.

Acknowledgments

This work was supported by the Czech Science Foundation (Project No. 104/07/1400) and by the Ministry of Education, Youth and Sports of the Czech Republic (Projects No. MSM 6046137302 and 6198910016). TEM was kindly performed by Jaroslav Boháček (Institute of Inorganic Chemistry ASCR).

References

[1] F. Cavani, F. Trifiro, A. Vaccari, Catal. Today 11 (1991) 173–301.
[2] F. Basile, A. Vaccari, in: V. Rives (Ed.), Layered Double Hydroxides: Present and Future, Nova Science Publishers, New York, 2001, pp. 285–321.
[3] F. Kovanda, K. Jirátová, R. Kalousková, in: F.L. Gerard (Ed.), Advances in Chemistry Research, vol. 1, Nova Science Publishers, New York, 2006, pp. 89–139.
[4] C. Qi, J.C. Amphlett, B.A. Peppley, Catal. Lett. 104 (2005) 57–62.
[5] B.M. Choudary, M.L. Kantam, A. Rahman, C.R.V. Reddy, J. Mol. Catal. A 206 (2003) 145–151.
[6] L. Obalová, K. Jirátová, F. Kovanda, M. Valášková, J. Balabánová, K. Pacultová, J. Mol. Catal. A 248 (2006) 210–219.
[7] T. Hibino, Y. Yamashita, K. Kosuge, A. Tsunashima, Clays Clay Miner. 43 (1995) 427–432.
[8] M. Bellotto, B. Rebours, O. Clause, J. Lynch, D. Bazin, E. Elkaim, J. Phys. Chem. 100 (1996) 8535–8542.
[9] E. Kanezaki, Inorg. Chem. 37 (1998) 2588–2590.
[10] T. Stanimirova, I. Vergilov, G. Kirov, N. Petrova, J. Mater. Sci. 34 (1999) 4153–4161.
[11] M. Jitianu, M. Balasoiu, R. Marchidan, M. Zaharescu, D. Crisan, M. Craiu, Int. J. Inorg. Mater. 2 (2000) 287–300.
[12] J. Pérez-Ramírez, G. Mul, J.A. Moulijn, Vib. Spectrosc. 27 (2001) 75–88.
[13] M. Jitianu, A. Jitianu, M. Zaharescu, D. Crisan, R. Marchidan, Vib. Spectrosc. 22 (2000) 75–86.
[14] S. Miyata, Clays Clay Miner. 28 (1980) 50–56.
[15] L. Hickey, J.T. Kloprogge, R.L. Frost, J. Mater. Sci. 35 (2000) 4347–4355.
[16] J.-M. Oh, S.-H. Hwang, J.-H. Choy, Solid State Ionics 151 (2002) 285–291.
[17] F. Kovanda, D. Koloušek, Z. Cílová, V. Hulínský, Appl. Clay Sci. 28 (2005) 101–109.
[18] S.K. Sharma, P.K. Kushwaha, V.K. Srivastava, S.D. Bhatt, R.V. Jasra, Ind. Eng. Chem. Res. 46 (2007) 4856–4865.
[19] O. Clause, M. Gazzano, F. Trifiro, A. Vaccari, L. Zatorski, Appl. Catal. 73 (1991) 217–236.
[20] F. Kooli, K. Kosuge, A. Tsunashima, J. Solid State Chem. 118 (1995) 285–291.
[21] M. del Arco, P. Malet, R. Trujillano, V. Rives, Chem. Mater. 11 (1999) 624–633.
[22] S. Möhmel, I. Kurzawski, D. Uecker, D. Müller, W. Gebner, Cryst. Res. Technol. 37 (2002) 359–369.
[23] P. Benito, F.M. Labajos, V. Rives, J. Solid State Chem. 179 (2006) 3784–3797.
[24] U. Costantino, F. Marmottini, M. Nocchetti, R. Vivani, Eur. J. Inorg. Chem. (1998) 1439–1446.
[25] P. Benito, M. Herrero, C. Barriga, F.M. Labajos, V. Rives, Inorg. Chem. 47 (2008) 5453–5463.
[26] P. Benito, I. Guinea, F.M. Labajos, V. Rives, J. Solid State Chem. 181 (2008) 987–996.
[27] E. Scavetta, A. Mignani, D. Prandstraller, D. Tonelli, Chem. Mater. 19 (2007) 4523–4529.
[28] F. Kovanda, T. Rojka, J. Dobešová, V. Machovič, P. Bezdička, L. Obalová, K. Jirátová, T. Grygar, J. Solid State Chem. 179 (2006) 812–823.
[29] C.-C. Yang, Int. J. Hydrogen Energy 27 (2002) 1071–1081.
[30] H.J. Scofield, J. Electron Spectrosc. Relat. Phenom. 8 (1976) 129–137.
[31] J. Pérez-Ramírez, S. Abelló, N.M. van der Pers, J. Phys. Chem. C 111 (2007) 3642–3650.
[32] K. Jirátová, P. Čuba, F. Kovanda, L. Hilaire, V. Pitchon, Catal. Today 76 (2002) 43–53.
[33] F. Trifiro, A. Vaccari, O. Clause, Catal. Today 21 (1994) 185–195.
[34] A.P. Grosvenor, M.C. Biesinger, R. St.C. Smart, N.S. McIntyre, Surf. Sci. 600 (2006) 1771–1779.
[35] L.M. Moroney, R.St.C. Smart, M.W. Roberts, J. Chem. Soc. Faraday Trans. 1 (79) (1983) 1769–1778.
[36] H.A.E. Hagelin-Weaver, J.F. Weaver, G.B. Hoflund, G.N. Salaita, J. Alloys Compd. 389 (2005) 34–41.
[37] H.S. Fogler, Elements of Chemical Reaction Engineering, third ed., Prentice-Hall PTR, New Jersey, 1999.